nature climate change

ARTICLES

PUBLISHED ONLINE: 3 AUGUST 2015 | DOI: 10.1038/NCLIMATE2729

Long-term response of oceans to CO_2 removal from the atmosphere

Sabine Mathesius[1,2*], Matthias Hofmann[1], Ken Caldeira[3] and Hans Joachim Schellnhuber[1,4]

Carbon dioxide removal (CDR) from the atmosphere has been proposed as a measure for mitigating global warming and ocean acidification. To assess the extent to which CDR might eliminate the long-term consequences of anthropogenic CO_2 emissions in the marine environment, we simulate the effect of two massive CDR interventions with CO_2 extraction rates of 5 GtC yr^{-1} and 25 GtC yr^{-1}, respectively, while CO_2 emissions follow the extended RCP8.5 pathway. We falsify two hypotheses: the first being that CDR can restore pre-industrial conditions in the ocean by reducing the atmospheric CO_2 concentration back to its pre-industrial level, and the second being that high CO_2 emissions rates (RCP8.5) followed by CDR have long-term oceanic consequences that are similar to those of low emissions rates (RCP2.6). Focusing on pH, temperature and dissolved oxygen, we find that even after several centuries of CDR deployment, past CO_2 emissions would leave a substantial legacy in the marine environment.

Averting dangerous climate change[1] is regarded as one of the greatest challenges for modern civilization. There is a scientific consensus that unbridled emissions of the long-lived[2,3] greenhouse gas CO_2 would substantially alter the planetary environment[4] and potentially threaten human livelihoods for centuries[5]. Therefore, so-called geoengineering measures have been proposed[6–8] to be implemented in case climate action fails to reduce emissions sufficiently fast.

One category of geoengineering schemes, solar radiation management, has the potential to cool the atmosphere quickly and at relatively low direct cost, yet may be highly risky[9]. A crucial shortcoming of solar radiation management is that it cannot reverse ocean acidification[10]. In contrast, carbon dioxide removal (CDR) is likely to reduce temperature anomalies rather slowly and at considerable cost[11], but could address the proximal cause of the problem, namely high atmospheric CO_2 concentrations. In this study, we first investigate the hypothesis that CDR has the potential to restore pre-industrial conditions in the marine environment by re-establishing the pre-industrial atmospheric CO_2 concentration of 280 ppm, after the system has been extensively exposed to a business-as-usual (RCP8.5) world[12]. Furthermore, we test the second hypothesis that delayed emissions reduction with following CDR deployment would result in a state similar to that predicted in the low-emissions RCP2.6 scenario[12]. Our results suggest that even a probably unfeasible CO_2 extraction rate of 25 GtC yr^{-1} could neither entirely re-establish pre-industrial conditions nor a state comparable to the RCP2.6 scenario, within the simulated period (until year 2700).

We conclude that CO_2 emission with subsequent CDR leaves a long-term legacy in the ocean, and thus CO_2 emissions with subsequent removal should not be considered the equivalent of an avoided emission[13].

Experimental design

Our three-dimensional Earth system model CLIMBER-3α-C (see Methods) has been forced with historic CO_2 emissions from 1800 to 2005; with a subsequent business-as-usual emissions scenario extending to 2150; and with linearly declining emissions afterwards, reaching a constant value of 2 GtC yr^{-1} in 2250 (extended RCP8.5 pathway[12]). We refer to this scenario as CDR0. In a first scenario set, CDR deployment starts in 2250, when the CO_2 emissions stabilize, to clearly distinguish the effect of CDR from the effect of emissions reduction. At the same time, the late onset leads to a strong anomaly signal that illustrates well the timescales and processes responsible for the analysed changes.

This first scenario set consists of a substantial CDR scheme (CDR5) with a maximum extraction rate of 5 GtC yr^{-1} (equivalent to 18.3 Gt CO_2 yr^{-1}, about half of present-day emissions) and an extreme CDR scheme (CDR25) with a maximum extraction rate of 25 GtC yr^{-1} (equivalent to 91.7 Gt CO_2 yr^{-1}). Although CDR25 can be regarded as unfeasible[11] it serves well as a thought experiment for exploring the limitations of CDR as a restoration strategy for the marine environment. In our simulations, the CO_2 extraction rate is gradually increased from 0.1 GtC yr^{-1} in 2250 to the respective upper limit over a period of approximately 100 years to emulate an increasing deployment (Table 1 and Fig. 1a).

The second set of experiments, for hypothesis 2, starts with CO_2 extraction of 5 GtC yr^{-1} (CDR5*) and 25 GtC yr^{-1} (CDR25*) in 2050 and 2150, respectively, without ramping in the deployment. The CDR25* scenario is subdivided into one scenario that brings atmospheric CO_2 down to 280 ppm and a second one that reduces CO_2 even further to 180 ppm, a concentration that was realized only during past glacial maxima[14]. Once the target level is reached, the CO_2 concentration is held constant.

In addition, we simulated a low-emissions scenario[12] (RCP2.6) for comparison with the modified RCP8.5 scenarios.

We consider CDR generically, without specifying any particular technique, yet we assume that the extracted CO_2 is taken out of the ocean–atmosphere system permanently (for example, stored underground).

Changes under RCP8.5 and impact of CDR

In the CDR0 baseline scenario, the CO_2 concentration reaches 2,100 ppm in year 2250 and stays almost constant for the remaining simulation period (Fig. 1b). This causes a persistent increase in

[1]Potsdam Institute for Climate Impact Research, PO Box 60 12 03, 14412 Potsdam, Germany. [2]GEOMAR Helmholtz Centre for Ocean Research Kiel, Düsternbrooker Weg 20, 24105 Kiel, Germany. [3]Department of Global Ecology, Carnegie Institution for Science, Stanford, California 94305, USA. [4]Santa Fe Institute, 1399 Hyde Park Road, Santa Fe, New Mexico 87501, USA. *e-mail: smathesius@geomar.de

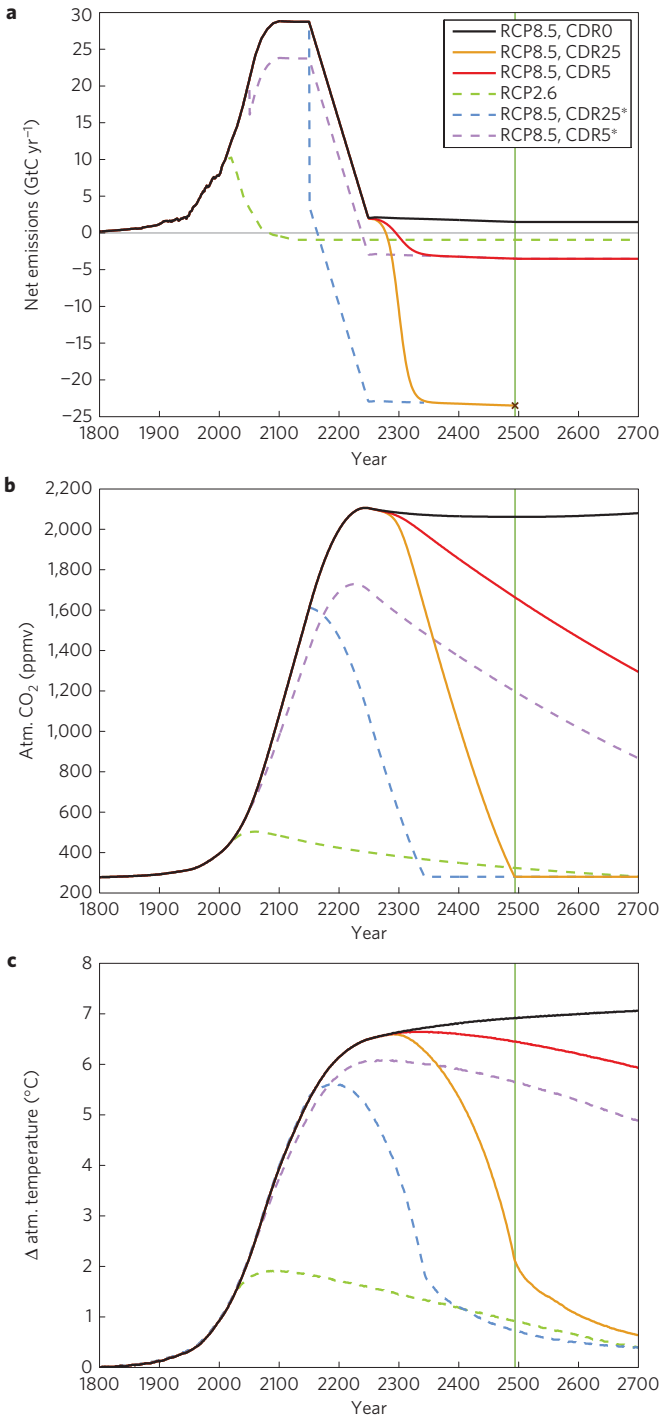

Figure 1 | Globally averaged atmospheric variables. Trajectories for RCP8.5 (black), CDR5 (red), CDR25 (orange), CDR5* (purple), CDR25* (blue) and RCP2.6 (green). See main text for further details. **a**, Net CO_2 emissions, defined as the CO_2 emissions minus the amount of CO_2 that is extracted. In the CDR25 scenario, the CO_2 concentration returns to 280 ppm shortly before 2500 (year 2494, vertical green line) and is held constant from then on, therefore no net emissions are presented for the remaining period. **b**, Atmospheric concentration of CO_2. **c**, Anomalies of atmospheric surface temperature, with respect to year 1800.

surface air temperature by up to 7.1 °C (Fig. 1c), an increase in sea surface temperature (SST) by 5.5 °C (Fig. 2b), an average warming of the entire ocean by 2.6 °C (Fig. 2e) and a thermosteric sea level rise on the order of 2 m (Supplementary Fig. 1). The dissolved oxygen (DO) concentration drops by up to 9% at the surface (Fig. 2c) and 16% in the interior ocean (Fig. 2f). The pH declines by 0.7 units at the surface (Fig. 2a) and by 0.3 units averaged over the entire ocean (Fig. 2d).

Recent CMIP5 studies[15,16] found the surface pH to be reduced by around 0.45 units in 2100, which is close to our reduction of 0.49 units. The range of SST increase in 2100 is around 2.5 to 4.2 °C in the CMIP5 studies. With 2.6 °C sea surface warming by 2100, our results are at the lower end of this range, possibly because our model is forced with CO_2 only, while the cited studies[15,16] partly took more greenhouse gases into account. For the average oxygen content, our model suggests a reduction by 5.5%, while the CMIP5 studies found the range between approximately 3.8% and 4.6%, by 2100.

In the CDR5 scenario, atmospheric CO_2 decreases by about 1.9 ppm yr^{-1} to 1,290 ppm in year 2700, with surface air temperatures still 5.9 °C above pre-industrial after more than 400 years of geoengineering (Fig. 1c). In contrast, in the CDR25 scenario, the atmospheric CO_2 concentration is restored to pre-industrial values by year 2500. By this time, a total of 5,835 GtC has been emitted and 4,861 GtC (83.3%) has been removed, while the remaining carbon has been taken up by the ocean (Supplementary Fig. 2). Although the pre-industrial CO_2 concentration is re-established, surface air temperatures are still elevated by 2.0 °C in 2500, and even after the atmospheric CO_2 has been at 280 ppm for 200 years, the temperatures of both the atmosphere and surface ocean are about 0.6 °C warmer than in pre-industrial times (Figs 1c and 2b,e, respectively).

The recovery in surface pH largely follows the atmospheric CO_2 reduction (Fig. 2a). However, the average pH of the entire ocean does not differ substantially in CDR5 from CDR0, and even in the CDR25 scenario does not closely approximate the pre-industrial state within the time span modelled (Fig. 2d). As with pH and temperature, surface dissolved oxygen concentrations recover substantially in both CDR scenarios. Even the average dissolved oxygen concentration of the entire ocean experiences some remediation under CDR5, and closely approaches the pre-industrial state under CDR25 (Fig. 2f). However, large areas of the upper ocean experience an increase in oxygen (Fig. 3i), partly counteracting the general decrease on global average and suggesting an overall lower impact and faster recovery of oxygen than in the case of pH and temperature. The maximum perturbation of oxygen concentration is higher in the entire ocean average than for the surface average—partly caused by positive surface oxygen anomalies that weaken the negative trend and at the same time resulting from severe deoxygenation of the deep ocean due to reduced ventilation, as discussed later in detail.

While globally averaged values indicate general trends, the spatial distribution of the anomalies provides important additional insights. Here we discuss the scenario-dependent anomalies of ocean pH, temperature and dissolved oxygen in a geographically explicit way for year 2500, when the CDR25 scenario returns to 280 ppm. All anomalies are relative to the pre-industrial state in year 1800 (Supplementary Fig. 3); for the depth-resolved temporal evolution of the anomalies see Supplementary Fig. 4.

The most severe acidification (as measured by pH changes) tends to occur at high latitudes (Fig. 3a), since cold water is characterized by a high solubility of CO_2. In CDR0, surface pH drops by 0.85 to 0.95 units at high northern latitudes and 0.66 to 0.73 units at high southern latitudes. However, at low latitudes, surface pH also decreases by 0.69 to 0.75 units, similar to the Southern Ocean. By this time, acidification has penetrated most of the South Atlantic and the entire Southern Ocean, leading to substantial shoaling of the water volume saturated with calcium minerals (Fig. 3a, dashed line), and subsequent corrosive conditions in high latitudes.

Heat enters the deep ocean particularly at the latitudinal bands of 40° S–60° S and 50° N–70° N (Fig. 3b), then spreads meridionally at

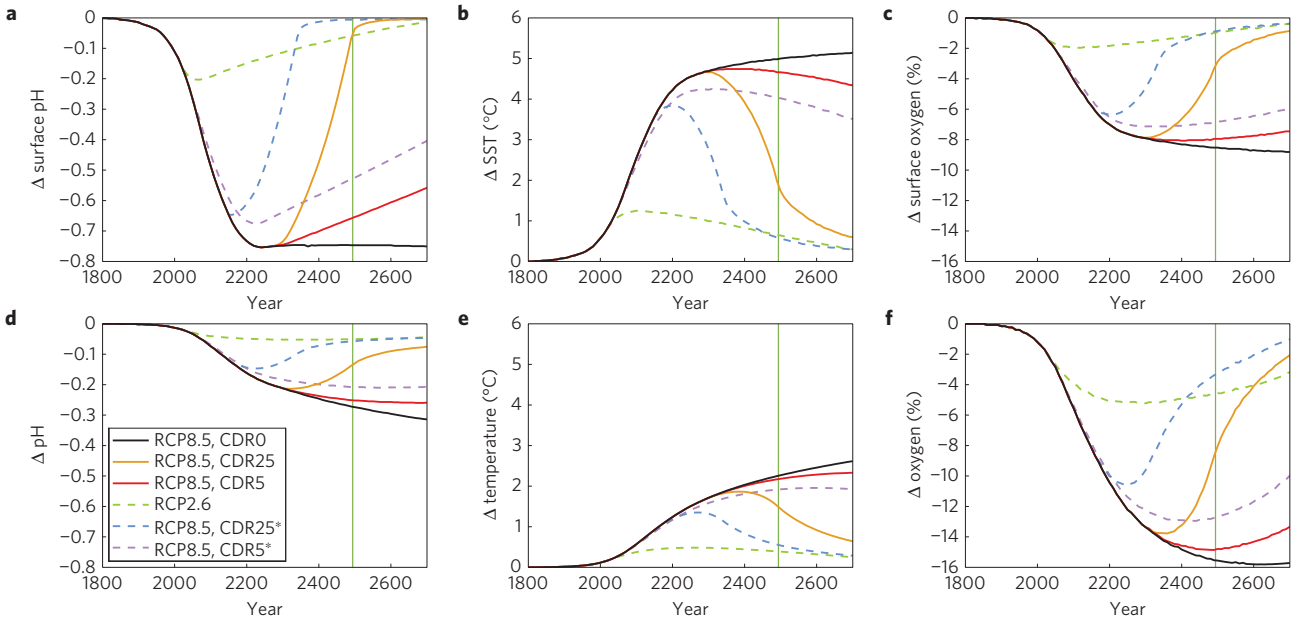

Figure 2 | Anomalies of globally averaged ocean variables for surface and entire ocean. a–f, Trajectories for RCP8.5 (black), CDR5 (red), CDR25 (orange), CDR5* (purple), CDR25* (blue), and RCP2.6 (green), showing globally averaged anomalies of surface pH (**a**), sea surface temperature (SST) (**b**), surface dissolved oxygen (**c**), entire ocean pH (**d**), entire ocean temperature (**e**) and entire ocean dissolved oxygen (**f**). The vertical green line marks the time when CDR25 reaches 280 ppm. All anomalies were calculated with respect to year 1800. Surface is defined as the ocean's upper 25 m.

Table 1 | Overview of simulated scenarios.

Scenario	Year of CDR onset	Max. CO_2 extraction rate	Extraction development
CDR0 (RCP8.5)	No CDR	–	–
CDR5	2250	5 GtC yr^{-1}	Logistically increasing extraction rate (see Methods; equation (1))
CDR25	2250	25 GtC yr^{-1}	Logistically increasing extraction rate (see Methods; equation (1))
CDR5*	2050	5 GtC yr^{-1}	Extraction immediately at maximum rate
CDR25*	2150	25 GtC yr^{-1}	Extraction immediately at maximum rate, until 280 ppm is reached
CDR25* (180 ppm)	2150	25 GtC yr^{-1}	Extraction immediately at maximum rate, until 180 ppm is reached
RCP2.6	No CDR	–	–

For each scenario, the table shows the year of CDR onset, the assumed upper limit of possible CO_2 extraction, and the way the extraction rate was increased over time. All CDR scenarios are imposed on the RCP8.5 scenario.

200–1,200 m depth, largely paralleling isopycnals, as has been shown previously[17]. Therefore, the strongest warming typically is not located at the surface but at the depth of intermediate waters[17]. In year 2500, averaged over the top 2,000 m of the ocean, the temperature increase relative to pre-industrial is 5.4 °C, locally exceeding 10 °C, while the water below is largely unaffected (Fig. 3b).

In most regions, the ocean also experiences severe oxygen depletion, especially in the 1,500–3,000 m depth range at mid and high latitudes (Fig. 3c). In contrast, we find an oxygen increase in intermediate waters of the tropics and polar regions (consistent with earlier studies[18]).

Despite the great effort[11] that would be required to extract 5 GtC yr^{-1}, the effect would be strikingly low compared to the magnitude of the anthropogenic changes. According to our simulations, in 2500, the zonally averaged pH is increased by less than 0.1 units, the temperature is reduced by less than 0.7 °C, and the effect on dissolved oxygen concentrations is almost negligible (Fig. 3d–f, respectively; Supplementary Fig. 5).

An extraction rate of 25 GtC yr^{-1} (CDR25) would have a substantial impact (Fig. 3g–i); yet even in this presumably unrealistic scenario pH, temperature and dissolved oxygen fields remain considerably altered, although atmospheric CO_2 has already returned to 280 ppm by 2500. By this time, the CDR impact can reach down to a depth of about 3,000 m in the high latitudes, but only down to a depth of about 2,000 m in the low latitudes (Supplementary Fig. 5). An extraction rate of 5 GtC yr^{-1} (CDR5) has a substantial effect in year 2500 down to about 2,000 m in the high latitudes and 1,000 m in the low latitudes.

In high-latitude deep-water formation zones, the 25 GtC yr^{-1} CDR scheme elevates the pH of the upper 2,000 m on average by 0.45 units with respect to CDR0, while in the more highly stratified low-latitude waters only the upper 1,000 m are substantially influenced, with pH values that are on average 0.38 units higher than in the CDR0 simulation; the influence of CDR diminishes with increasing depth. Despite this substantial intervention effect, the highest remaining acidification is still 0.2 to 0.3 pH units, primarily persisting in the 300–3,000 m depth zone (Fig. 3g).

In the upper 1,500 m, the average temperature is decreased by 2.1 °C relative to the CDR0 scenario, but is still 3.3 °C above the pre-industrial value (Fig. 3h). The heat flux from ocean to atmosphere is 2.8 W m^{-2} at this time (Supplementary Fig. 6). This is equivalent to the radiative forcing of 470 ppm CO_2—that is, although the actual CO_2 concentration has already returned to 280 ppm, the atmosphere still receives an energy input from the warmer ocean that is comparable to that of high atmospheric CO_2 concentrations.

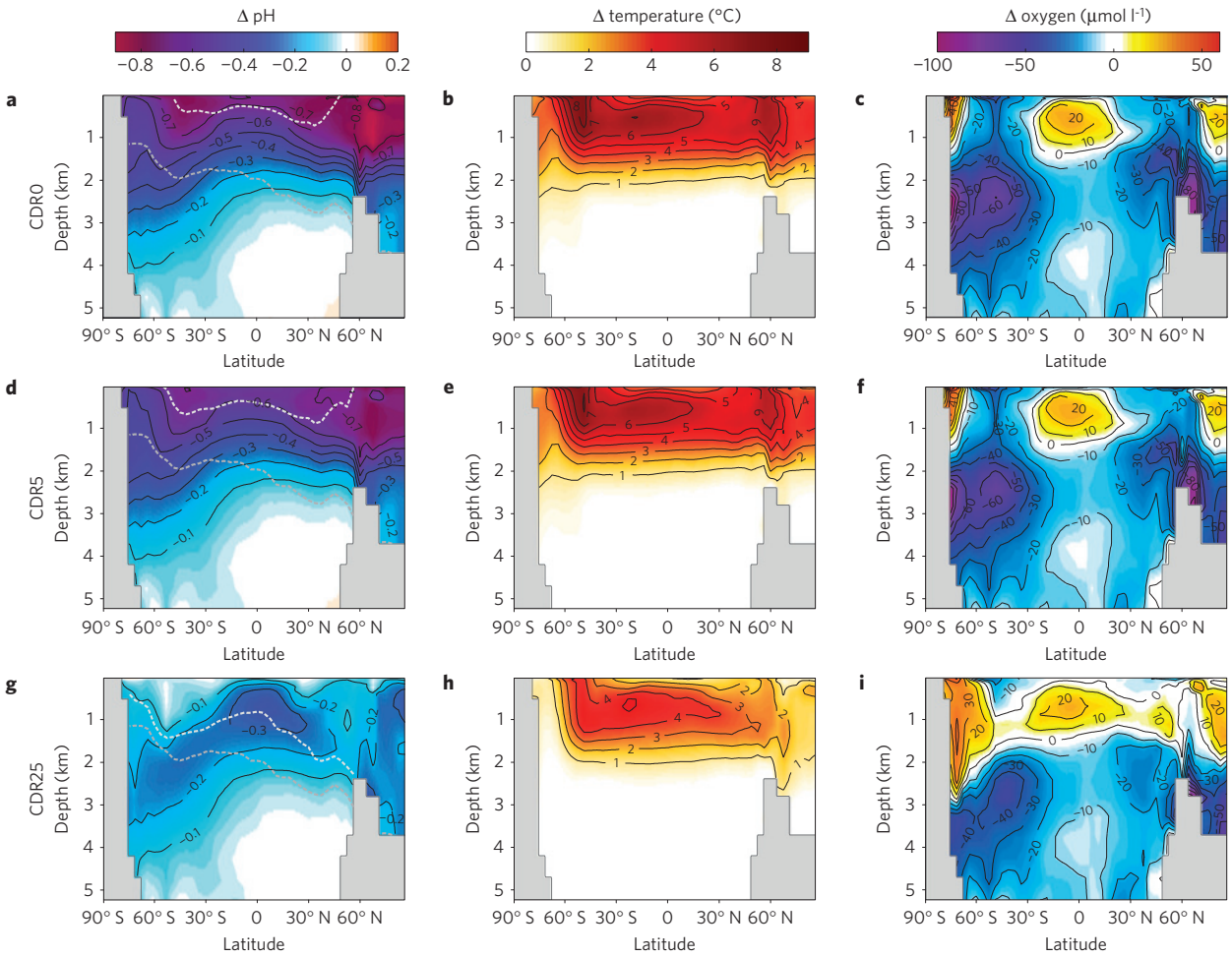

Figure 3 | Zonally averaged anomalies of pH, temperature and dissolved oxygen, in year 2500. a–c, Zonal-mean anomalies of pH (**a**), temperature (**b**) and dissolved oxygen (**c**) under RCP8.5. **d–f**, Same but for CDR5. **g–i**, Same but for CDR25. All anomalies were calculated with respect to year 1800. Grey shaded areas show the ocean's topography. The dashed lines show the calcite compensation depth for pre-industrial conditions (grey) and for the state in 2500 (white) for RCP8.5, CDR5, and CDR25, in **a**,**d**,**g**, respectively.

CDR25 has a major effect on dissolved oxygen concentrations in vast parts of the ocean, practically reversing depletion in the upper 1,500 m and enhancing already existing positive dissolved oxygen anomalies in the polar regions (Fig. 3i). The overturning circulation in 2500 is still shallower but in large regions stronger than in the pre-industrial state, primarily in the Northern Hemisphere (Supplementary Fig. 9), inducing higher ventilation and a general increase in dissolved oxygen. The mixed layer depth increases as well (Supplementary Fig. 7), especially in the Southern Ocean, and so does the vertical extent of the oxygen-enriched water.

The anomaly patterns of pH, temperature and dissolved oxygen presented here are shaped by a multitude of interlinked, yet totally distinct processes. However, pH is not strongly influenced by climate change, but primarily determined by atmospheric CO_2 changes, the CO_2 transport into the ocean and the slow ocean turnover, leading to a slow response of deep ocean pH to atmospheric CO_2 changes.

In contrast, the concentration of dissolved oxygen is mainly determined by the interplay of temperature, ocean circulation, primary and export production, and remineralization[15,16,19]. The increase in temperature reduces the solubility of oxygen, thereby decreasing concentrations at the surface, and at the same time enhances stratification, which in turn hampers deep ocean ventilation. Furthermore, stronger stratification suppresses the upward transport of nutrient-rich water, reducing primary production at the surface and related export production, and therefore also decreasing oxygen-consuming remineralization of exported organic matter in the water below (consistent with findings of earlier studies[20]). The latter mechanism contributes substantially to the simulated oxygen increase in the tropics and the Arctic Ocean, which are both regions of high primary and export production before anthropogenic change. Contrary to the overall decrease in phytoplankton (about 10% on global average), the abundance increases by more than 30% in the Southern Ocean (Supplementary Fig. 7), which increases dissolved oxygen concentrations at the surface through enhanced photosynthesis (Supplementary Fig. 8). The latter process also mitigates, to a limited extent, local acidification trends through CO_2 consumption (Supplementary Fig. 8).

The reduced deep convection in polar regions causes a weakening of North Atlantic Deep Water (NADW) and Antarctic Bottom Water (AABW) formation (see Supplementary Fig. 9), hampering the ventilation of the deep ocean. Altogether, increased stratification in combination with weaker meridional overturning intensifies the separation between the upper and deep ocean water masses, thus prolonging the equilibration time of the deep ocean with the atmosphere; this increased isolation would also hinder CDR efforts to restore pre-industrial pH at great depths.

Strong mitigation versus RCP8.5 with CDR

Above, we showed that once the ocean is severely affected by high CO_2, it is virtually impossible to undo these alterations

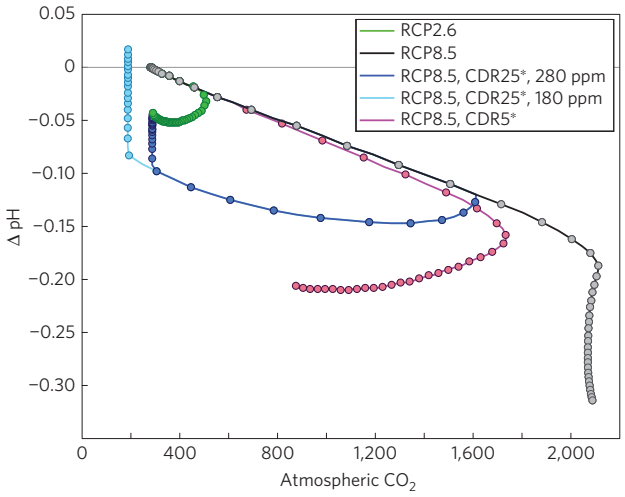

Figure 4 | Globally averaged pH anomalies as a function of atmospheric CO_2 concentration. Illustrated are the trajectories for RCP2.6 (green), RCP8.5 (black), CDR5* (purple) and CDR25* with CO_2 removal until the pre-industrial level of 280 ppm is restored (dark blue), and CDR25* with CO_2 removal until the glacial level of 180 ppm is reached (light blue), respectively. In both CDR25* scenarios CDR starts in 2150, while in CDR5* it begins already in 2050. Dots mark intervals of 20 years, indicating the rate of changes. All anomalies were calculated with respect to year 1800.

on a human-generation timescale. Equally interesting is whether a state similar to a low-emissions scenario could be achieved (hypothesis 2). We examine this using the example of pH, based on the RCP2.6 scenario and the second set of CDR scenarios that start with 5 GtC yr^{-1} and 25 GtC yr^{-1} CO_2 extraction in years 2050 and 2150, respectively. The early CDR scenarios produce anomaly patterns similar to those of the late CDR scenarios discussed above, but the maximum CO_2 increase is lower, and therefore the anomalies of all variables are weaker (see Figs 1 and 2).

Figure 4 first reveals, once again, the enormous excursion of the oceans' pH triggered by anthropogenic CO_2 emissions (Fig. 1, black line)—at an atmospheric CO_2 concentration of roughly 2,100 ppm, as projected in RCP8.5 for the year 2700, the magnitude of the globally averaged pH anomaly would exceed −0.3 units. A much smaller deviation results from the strong-mitigation scenario (RCP2.6; Fig. 1). Second, our simulations demonstrate that a CO_2 removal of 5 GtC yr^{-1} has only a modest effect on average marine pH as long as high emissions persist in the RCP8.5 background scenario—that is, until 2150. Even after the emissions have been reduced to a minimum of about 2 GtC yr^{-1}, ocean acidification is hardly reversed by that intervention, but merely 'stabilized', within our simulation period, at 0.2 pH units below pre-industrial (Fig. 1).

Third, the removal of 25 GtC yr^{-1} in both scenarios (280 ppm CO_2 end-point concentration and 180 ppm CO_2 end-point concentration) does result in a substantial recovery of mean oceanic pH. However, even under these extreme interventions, it takes several centuries to approach the average pH values of the RCP2.6 scenario. If atmospheric CO_2 were eventually reduced to the glacial level of 180 ppm, the convergence would be achieved in 2410, after 260 years of permanent CO_2 extraction at a massive scale. If CO_2 is reduced to pre-industrial 280 ppm, the average pH asymptotically approaches the average pH of the RCP2.6 scenario by about 2500. While acidity values at the sea surface recover nearly instantaneously when atmospheric CO_2 levels are geoengineered back to pre-industrial levels, the vast deep ocean remembers past human interference for several centuries, at least.

There is, however, another trait of CDR impact on pH that needs to be emphasized: for many ecosystems, not just the acidification at a given point in time is relevant, but also the preceding changes and the rates at which they occurred[21]. When strong mitigation is pursued—that is, avoidance of emissions according to RCP2.6—the acidification proceeds relatively slowly and becomes almost stable after 2200. In the RCP8.5/180 ppm-end-point scenario, however, marine pH is modified at a much faster rate. The pH value decreases rapidly until 2150, with a reduction of more than 0.5 units at the surface; the subsequent recovery occurs at a similar pace in the upper ocean, while the waters below 2,000 m remain largely unaffected by the CDR intervention. Around the year 2350, when the atmospheric CO_2 concentration falls below 280 ppm, the upper ocean starts to become more alkaline than it was in the pre-industrial state. While Fig. 4 shows that the global mean acidity values in the 180 ppm-end-point extraction scenario can reach the pH levels of the strong-mitigation scenario (RCP2.6), the final spatially explicit state of the oceans differs substantially between the two cases (Supplementary Fig. 10; see Supplementary Fig. 11 for the 280 ppm scenario). In fact, pH in huge upper parts of the ocean is forced above pre-industrial levels (since the atmospheric CO_2 concentration is forced below the pre-industrial value), whereas the deeper ocean remains significantly acidified. Those anomalies cancel each other only on average to restore the mean pH value, yet would most likely constitute challenging environmental conditions individually. In the RCP2.6 scenario, the oceans are widely acidified as well, but the range of pH anomalies is narrower and the deviation field is distributed much more homogeneously (see also Fig. 5).

Marine changes of the magnitude discussed here have been associated with mass extinctions in the past[21,22] and could threaten marine ecosystems in the future[16,23,24]. Ocean acidification in combination with heat stress and expanding dead zones—phenomena already observed[25,26]—would exert a dangerous complex of pressures on some marine ecosystems. Rapidly undoing ocean acidification could conceivably pose challenges for many ecosystems, if it occurred after intermediate adaptation of organisms to acidified environments, since the surviving species would have to re-adapt to a then more alkaline environment, in a rather short period of time. While many organisms are expected to have difficulties in coping with ocean acidification[27,28] and the associated changes in ecosystems structure[29], a brutal shift back to the original environment would create yet another selection pressure, potentially further diminishing biodiversity and resilience.

Timescales of ocean recovery

In an early study by Hasselmann and Maier-Reimer[30] it was shown that the large-scale ocean dynamics can be divided into processes mainly operating at three different timescales. While atmospheric dissolution of CO_2 combined with mixing in the upper ocean tends to operate on a decadal timescale, processes tied to the intermediate and deep ocean are associated with multidecadal to multi-centennial or even millennial[31] residence timescales, respectively. The latter can be attributed to the large-scale thermohaline circulation of the ocean[32], characterized by an overturning timescale of about 1,000 years. These findings are consistent with our simulations. While surface properties after the deployment of CDR25 recover rapidly towards pre-industrial conditions (Fig. 2a–c), the deep ocean will not achieve this state even at the end of our simulations (year 2700; Fig. 2d–f).

Increased stratification and reduced overturning circulation (Supplementary Fig. 9) will lead to an isolation of the deep ocean; these factors would tend to prolong the deep ocean 'memory' of anthropogenic changes. In summary, the longevity of the anthropogenic signal in the deep ocean found in our study is mainly a feature of the intercommunication timescales of the different water masses (surface, intermediate, and deep waters) and does not depend on the specific emission scenario or model used, underlining the robustness of our results.

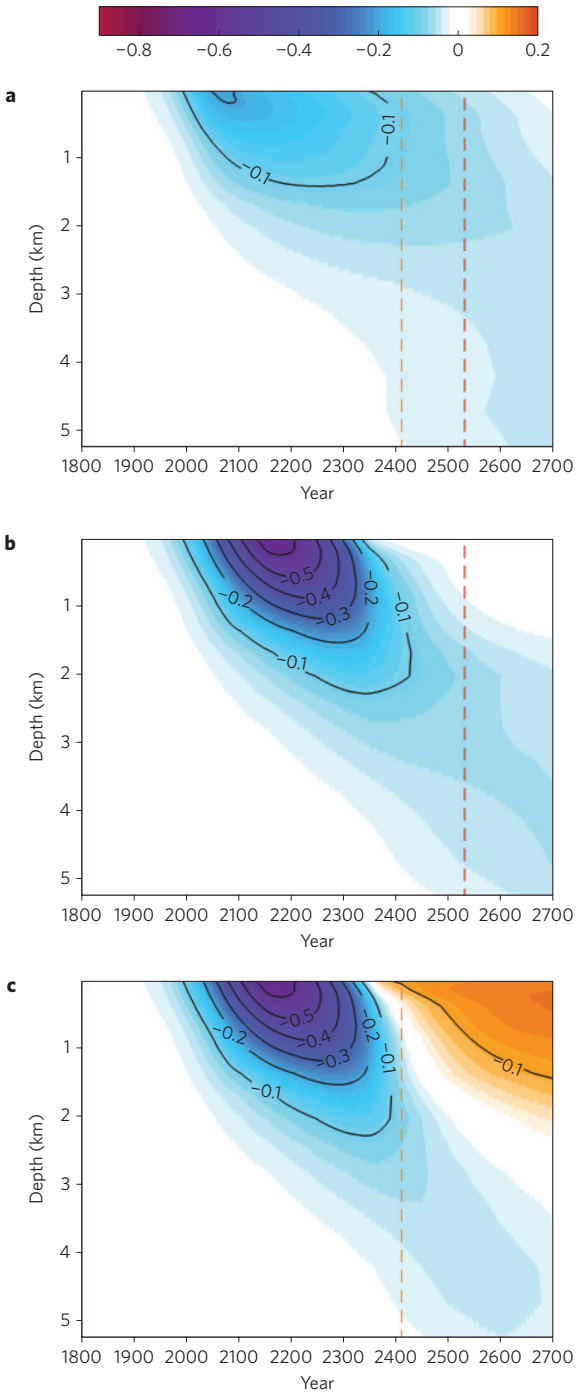

Figure 5 | Depth-resolved evolution of zonally averaged pH anomalies. **a**–**c**, Temporal evolution of zonal-mean pH anomalies for RCP2.6 (**a**), CDR25* until the atmospheric CO_2 concentration of 280 ppm is reached (**b**), and CDR25* until the atmospheric CO_2 concentration of 180 ppm is reached (**c**). The vertical lines mark the time when the zonal-mean pH of CDR25*/280 ppm (red dashed) and CDR25*/180 ppm (orange dashed), respectively, is the same as the zonal-mean pH of the RCP2.6 scenario. All anomalies were calculated with respect to the pre-industrial state in year 1800.

Conclusion

Our study clearly shows that if the global community follows a business-as-usual CO_2 emissions scenario into the future, even massive deployment of CDR schemes cannot reverse the substantial impacts of these emissions on the marine environment on the multi-centennial timescale. Furthermore, it would not be possible for CDR to transform the RCP8.5 ocean into an RCP2.6 ocean on the multi-century timescale considered here. The implementation of the 25 GtC yr^{-1} scheme appears to be beyond all operational and socioeconomic reach[33], yet, even at this high level of effort, a substantial legacy of anthropogenic CO_2 emissions would persist in the oceans far into the future.

The deep ocean's pH could be restored only if the pertinent water masses come into close contact with the remediated atmosphere again, which could take several millennia[32].

Thus, the slow ocean turnover hampers any CDR attempts to return the ocean's interior to the pre-industrial or an RCP2.6 state, regardless of the extraction rate.

Independent of the question whether a return to pre-industrial conditions would be possible, it is reasonable to assume that marine organisms would experience further stress instead of relief if they were forced to re-adapt to pre-industrial conditions.

Thus, our findings contribute to the growing body of evidence[5,11,12,34,35] supporting the view that immediate and ambitious action to reduce CO_2 emissions is the most reliable strategy for avoiding dangerous climate change, ocean acidification, and large-scale threats to marine ecosystems.

Methods

Methods and any associated references are available in the online version of the paper.

Received 10 December 2014; accepted 19 June 2015; published online 3 August 2015

References

1. Schellnhuber, H. J. *et al.* (eds) *Avoiding Dangerous Climate Change* (Cambridge Univ. Press, 2006).
2. Archer, D. & Brovkin, V. Millennial atmospheric lifetime of anthropogenic CO_2. *Climatic Change* **90,** 283–297 (2008).
3. Allen, M. R. *et al.* Warming caused by cumulative carbon emissions towards the trillionth tonne. *Nature* **458,** 1163–1166 (2009).
4. IPCC *Climate Change 2013: The Physical Science Basis* (eds Stocker, T. F. *et al.*) (Cambridge Univ. Press, 2013).
5. IPCC *Climate Change 2014: Impacts, Adaptation, and Vulnerability* (eds Field, C. B. *et al.*) (Cambridge Univ. Press, 2014).
6. Caldeira, K., Bala, G. & Cao, L. The Science of geoengineering. *Annu. Rev. Earth Planet. Sci.* **41,** 231–256 (2013).
7. Cao, L. & Caldeira, K. Atmospheric carbon dioxide removal: Long-term consequences and commitment. *Environ. Res. Lett.* **5,** 024011 (2010).
8. Vaughan, N. E. & Lenton, T. M. A review of climate geoengineering proposals. *Climatic Change* **109,** 745–790 (2009).
9. National Research Council *Climate Intervention: Reflecting Sunlight to Cool Earth* (The National Academies Press, 2015).
10. Matthews, D. L., Cao, L. & Caldeira, K. Sensitivity of ocean acidification to geoengineered climate stabilization. *Geophys. Res. Lett.* **36,** L10706 (2009).
11. National Research Council *Climate Intervention: Carbon Dioxide Removal and Reliable Sequestration* (The National Academies Press, 2015).
12. Meinshausen, M. *et al.* The RCP greenhouse gas concentrations and their extension from 1765 to 2300. *Climatic Change* **109,** 213–241 (2011).
13. Pielke, R. Jr. Air capture update. *Nature Geosci.* **2,** http://dx.doi.org/10.1038/ngeo690 (2009).
14. Petit *et al.* Climate and atmospheric history of the past 420,000 years from the Vostok ice core, Antarctica. *Nature* **399,** 429–436 (1999).
15. Bopp, L. *et al.* Multiple stressors of ocean ecosystems in the 21st century: Projections with CMIP5 models. *Biogeosci. Discuss.* **10,** 3627–3676 (2013).
16. Cocco, V. *et al.* Oxygen and indicators of stress for marine life in multi-model global warming projections. *Biogeosciences* **10,** 1849–1868 (2013).
17. Schewe, J., Levermann, A. & Meinshausen, M. Climate change under a scenario near 1.5 °C of global warming: Monsoon intensification, ocean warming and steric sea level rise. *Earth Syst. Dyn.* **2,** 25–35 (2011).
18. Matear, R. J. & Hirst, A. C. Long-term changes in dissolved oxygen concentrations in the ocean caused by protracted global warming. *Glob. Biogeochem. Cycles* **17,** 1125 (2003).
19. Matear, R. J., Hirst, A. C. & McNeil, B. I. Changes in dissolved oxygen in the Southern Ocean with climate change. *Geochem. Geophys. Geosyst.* **1,** 2000GC000086 (2000).

20. Hofmann, M., Worm, B., Rahmstorf, S. & Schellnhuber, H. J. Declining ocean chlorophyll under unabated anthropogenic CO_2 emissions. *Environ. Res. Lett.* **6,** 034035 (2011).
21. Guinotte, J. M. & Fabry, V. J. Ocean acidification and its potential effects on marine ecosystems. *Ann. N. Y. Acad. Sci.* **1134,** 320–342 (2008).
22. Penman, D. E., Hönisch, B., Zeebe, R. E., Thomas, E. & Zachos, J. C. Rapid and sustained surface ocean acidification during the Paleocene–Eocene Thermal Maximum. *Paleoceanography* **29,** 357–369 (2014).
23. Jackson, J. B. C. Ecological extinction and evolution in the brave new ocean. *Proc. Natl Acad. Sci. USA* **105,** 11458–11465 (2008).
24. Gruber, N. Warming up, turning sour, losing breath: Ocean biogeochemistry under global change. *Phil. Trans. R. Soc. A* **369,** 1980–1996 (2011).
25. Bednarsek, N. *et al.* Murphy Extensive dissolution of live pteropods in the Southern Ocean. *Nature Geosci.* **5,** 881–885 (2012).
26. Eakin, C. M. *et al.* Caribbean Corals in crisis: Record thermal stress, bleaching, and mortality in 2005. *PLoS ONE* **5,** e13969 (2010).
27. Wittmann, A. C. & Pörtner, H. Sensitivities of extant animal taxa to ocean acidification. *Nature Clim. Change* **3,** 995–1001 (2013).
28. Hofmann, M. & Schellnhuber, H. J. Ocean acidification: A millennial challenge. *Energy Environ. Sci.* **3,** 1883–1896 (2010).
29. Veron, J. E. N. *et al.* The coral reef crisis: The critical importance of <350 ppm CO_2. *Mar. Pollut. Bull.* **58,** 1428–1436 (2009).
30. Maier-Reimer, E. & Hasselmann, K. Transport and storage of CO_2 in the ocean—an inorganic ocean-circulation carbon cycle model. *Clim. Dynam.* **2,** 63–90 (1987).
31. Eby, M. *et al.* Historical and idealized climate model experiments: An intercomparison of Earth system models of intermediate complexity. *Clim. Past* **9,** 1111–1140 (2013).
32. Rahmstorf, S. Ocean circulation and climate during the past 120,000 years. *Nature* **419,** 207–214 (2002).
33. Caldecott, B. L., Lomax, G. & Workman, M. *Stranded Carbon Assets and Negative Emissions Technologies* (*NETs*) (Smith School of Enterprise and Environment, Working Paper Series, Univ. Oxford, 2015).
34. Cao, L., Han, Z., Meidi, Z. & Shuangjing, W. Response of ocean acidification to a gradual increase and decrease of atmospheric CO_2. *Environ. Res. Lett.* **9,** 024012 (2014).
35. Schellnhuber, H. J. Geoengineering: The good, the MAD, and the sensible. *Proc. Natl Acad. Sci. USA* **108,** 20277–20278 (2011).

Acknowledgements

Computational resources were provided by the Potsdam Institute for Climate Impact Research (PIK). CO_2 emission data were provided by M. Meinshausen from PIK, downloaded from his website: http://www.pik-potsdam.de/~mmalte/rcps.

Author contributions

H.J.S. conceived and designed the study with S.M., M.H. and K.C. M.H. coupled the EMIC CLIMBER-3α with the biogeochemical model and S.M. wrote the CDR code. S.M. carried out the simulations, analysed the results and produced the figures under the guidance of M.H., K.C. and H.J.S. S.M. wrote the first draft and all authors made contributions to writing the manuscript.

Additional information

Supplementary information is available in the online version of the paper. Reprints and permissions information is available online at www.nature.com/reprints. Correspondence and requests for materials should be addressed to S.M.

Competing financial interests

The authors declare no competing financial interests.

Methods

Model. In our study, we have employed a global three-dimensional Earth System Model of Intermediate Complexity[36]—CLIMBER-3α (ref. 37)—in a version running with a coupled prognostic model of the global marine carbon cycle[38]. CLIMBER-3α uses a coarse-resolution version of the Modular Ocean Model, version 3.0 (MOM-3 (ref. 39)) with a horizontal resolution of 3.75° × 3.75° and 24 vertical levels with thickness increasing from 25 m at the top to 500 m at the bottom. The ocean model is coupled interactively to a statistical dynamical atmospheric model which does not resolve synoptic scale processes (POTSDAM-2 (ref. 40)), and a dynamic-thermodynamic sea-ice model[41] based on the elasto-viscous-plastic rheology. While the sea-ice model utilizes the same horizontal resolution as the ocean, the resolution of the atmosphere is 22.5° in longitude and 7.5° in latitude.

The implementation of the global ocean carbon cycle is based on HAMOCC-3.1 (ref. 42), simulating the dynamics of dissolved inorganic carbon, total alkalinity, phosphate, oxygen, silicate, phytoplankton, zooplankton, particulate organic carbon, particulate inorganic carbon (calcite), and dissolved organic carbon. The kinetics of the underlying biogeochemical processes is derived from the assumption of a fixed elemental stoichiometry (Redfield ratio). Since we do not account for losses of matter to the bottom by sediment accumulation and burial, the model is isogeochemical. Phytoplankton growth rates are parameterized as a function of the photosynthetically available radiation (PAR), temperature and mixed layer depth. Phosphate is assumed to be the only growth-limiting nutrient. Below the 100 m depth horizon, sedimentation fluxes of particulate organic/inorganic carbon and opal follow an exponentially shaped profile, assuming an e-folding penetration depth of 1,000 m and 12,000 m, respectively. Because the model does not include an iron cycle, phytoplankton growth rates have been scaled by a factor of 0.25 everywhere in the ocean south of 30° S to emulate iron limitation in the Southern Ocean. Phytoplankton is consumed by zooplankton (grazing) at a temperature-dependent rate. The gas transfer of carbon dioxide between the ocean and the atmosphere was treated as a quadratic function of the 10-m-height wind speed[43]. To account for a slight numerical mass leakage observed in the model's carbon budget, a fixed carbon flux to the ocean–atmosphere system of 0.15 GtC yr^{-1} is added.

The model does not include freshwater input from melting land ice and, therefore, is likely to underestimate stratification under global warming. The warming-induced increase in primary production in polar regions is probably overestimated in our simulations, because the model does not account for phytoplankton and algae growing under sea ice, thus the productivity rapidly increases when sea ice retreats.

The model's pre-industrial patterns of ocean pH, temperature and oxygen compare reasonably well with observational data (see Supplementary Fig. 3). The performance of the physical part of CLIMBER-3α (without the marine carbon cycle) regarding the reproducibility of the current climate and the reliability of future projections has been frequently evaluated in several model intercomparison studies (EMIC/CMIP/PMIP; refs 31,44–46). It has been found that all of the simulation results provided by employing CLIMBER-3α are consistent with EMIC-based multi-model assessments.

When subjecting the model to anthropogenic CO_2 emissions following the RCP8.5 scenario, the drop in global ocean surface pH amounts to about 0.45 units in year 2100, a value comparable to the conclusions by the Fifth Assessment Report (AR5) of the IPCC[4] (see Figure SPM.7 in the Summary for Policymakers of AR5). In a recent work[47], employing the University of Victoria model (UVic), the authors found a sea surface reduction in pH by about 0.7 units and a global ocean pH drop by about 0.6 units when extending the simulations until year 2500. This response is similar to our findings (see our Fig. 2a,d in comparison to Fig. 2b,h in Cao and colleagues[47]). Furthermore the decline in the sea surface and global ocean oxygen concentrations are also of the same magnitude as in our study (see our Fig. 2c,f in comparison to Fig. 2f,l in Cao and colleagues[47]).

Study design. The different CDR scenarios are imposed on the extended RCP8.5 scenario from Meinshausen *et al.*[12]. The model is forced with CO_2 emission data, consisting of fossil and industrial CO_2 emissions as well as land-use-related CO_2 emissions (data downloaded from http://www.pik-potsdam.de/~mmalte/rcps). After year 2500, we extended this emission scenario further until year 2700 with a persistent CO_2 emission level of 1.5 GtC yr^{-1}.

The CO_2 extraction starts in year 2250, when the emissions reach a low level of non-mitigable CO_2 emissions (1.5 to 2.1 GtC yr^{-1}). Both CDR scenarios presented in this paper are based on logistic functions in the form of equation (1).

$$f(t) = L \frac{1}{1 + e^{(-nLt)} \times \left(\frac{L}{0.1} - 1\right)} \quad (1)$$

where t is the time, L is the upper limit of the respective CDR scenario (5 GtC yr^{-1} and 25 GtC yr^{-1}, respectively), and n is a factor that influences the slope of the function's curve, defined such that 50% of the upper limit is reached after 50 years (15.57×10^{-3} and 4.41×10^{-3}, respectively).

In the second set of experiments, CDR deployment is not assumed to follow a logistic function, instead we apply constant CO_2 removal rates of 5 and 25 GtC yr^{-1}, starting in 2050 and 2150, respectively. Like for RCP8.5, CO_2 emissions data for the simulated RCP2.6 scenario were provided by Meinshausen and colleagues[12].

When the atmospheric CO_2 concentration reaches the pre-industrial level of 280 ppm in our simulation, it is held constant at that level. This can be interpreted as a continued CO_2 extraction that is perfectly adjusted to the remaining CO_2 sources, such as oceanic outgassing and continued non-mitigable emissions.

Calculations. The presented (spatial) anomalies were calculated by subtracting the (zonally) averaged values of the pre-industrial control run from the (zonally) averaged values of the CDR runs and RCP runs. In the case of pH, due to its logarithmic nature, the average was obtained by first calculating the hydrogen ion concentration, then averaging the hydrogen ion concentration, and finally translating the result back to pH by taking the decimal logarithm of the reciprocal average hydrogen ion concentration.

References

36. Claussen, M. *et al.* Earth system models of intermediate complexity: Closing the gap in the spectrum of climate system models. *Clim. Dynam.* **18,** 579–586 (2002).
37. Montoya, M. *et al.* The Earth system model of intermediate complexity CLIMBER-3α. Part I: Description and performance for present-day conditions. *Clim. Dynam.* **25,** 237–263 (2005).
38. Brovkin, V., Kim, J.-H., Hofmann, M. & Schneider, R. A lowering effect of reconstructed Holocene changes in sea surface temperatures on the atmospheric CO_2 concentration. *Glob. Biogeochem. Cycles* **22,** GB1016 (2008).
39. Pacanowski, R. C. & Griffies, S. M. *The MOM-3 Manual Technical Report* 4 (GFDL Ocean Group, NOAA/Geophysical Fluid Dynamics Laboratory, 1999).
40. Petoukhov, V. *et al.* CLIMBER-2: A climate system model of intermediate complexity Part I: Model description and performance for present climate. *Clim. Dynam.* **16,** 1–17 (2000).
41. Fichefet, T. & Maqueda, M. A. M. Sensitivity of a global sea ice model to the treatment of ice thermodynamics. *J. Geophys. Res.* **102,** 12,609–12,646 (1997).
42. Six, K. & Maier-Reimer, E. Effects of phytoplankton on seasonal carbon fluxes in an ocean general circulation model. *Glob. Biogeochem. Cycles* **10,** 559–583 (1996).
43. Wanninkhof, R. Relationship between wind speed and gas exchange over the ocean. *J. Geophys. Res.* **97,** 7373–7382 (1992).
44. Stouffer, R. J. *et al.* Investigating the causes of the response of the thermohaline circulation to past and future climate changes. *J. Clim.* **19,** 1365–1387 (2006).
45. Gregory, J. M. A model intercomparison of changes in the Atlantic thermohaline circulation in response to increasing atmospheric CO_2 concentration. *Geophys. Res. Lett.* **32,** 1365–1387 (2005).
46. Petoukhov, V. *et al.* EMIC Intercomparison Project (EMIP–CO_2): Comparative analysis of EMIC simulations of climate, and of equilibrium and transient responses to atmospheric CO_2 doubling. *Clim. Dynam.* **25,** 363–385 (2005).
47. Cao, L. *et al.* Sensitivity of ocean acidification and oxygen to the uncertainty in climate change. *Environ. Res. Lett.* **9,** 064005 (2014).